Color Estimation from a Single Surface Color

Rei Kawakami and Katsushi Ikeuchi
Institute of Industrial Science, The University of Tokyo
{rei,ki}@cvl.iis.u-tokyo.ac.jp

Abstract

This paper estimates illumination colors by using only a single surface color taken under multiple illumination colors. Past researchers have found that there is a difficulty in estimating illumination colors using a single surface color. However, the method presented here overcomes the problem. Surface color is estimated by considering four characteristics of illumination and surface color spaces. First, the outdoor-illumination colors exist in a specific color range. Second, multiple illuminations give constraints for the surface color. Third, multiple illuminations also give constraints for the color range. Fourth, each color component affects those constraints in a different manner. Based on those characteristics, a novel method can be designed. The proposed method produces consistently accurate results when multiple illumination colors are used, because the constraint (possible range of illumination colors) on illumination colors refines the estimated illumination colors, effectively.

1. Introduction

Acquiring an object's inherent color is important when modeling a real-world object. Since color appearance varies by its illumination color, a method to remove it and to estimate the actual color of the object's surface is required. It is the goal of this work to estimate surface color, the object's color under white illumination.

An automatic white balance, specifically called color constancy in the field of computer vision, has been intensively studied; however, none of them can perform perfect color constancy. Depending on the target object, we can categorize methods into two groups: dichromatic-based and diffuse-based methods. The former methods use the presence of highlighting [4, 16, 26, 24]. They are accurate though less applicable to many outdoor objects. Methods that handle diffuse objects are further categorized into two groups [11]: algorithms that use information from a learning phase [9, 20, 2, 23, 8, 25, 5] and those based on low-level image features [3, 15, 27, 10]. Both methods explicitly assume that the scene contains a variety of surface colors, and the illumination color is uniform.

This paper tackles a difficult issue to estimate illumination colors with a single surface color. We assume that the scene contains a single surface color but can be observed under multiple illuminations. This enable us to perform a pixel-based operation. There have been discussions about the physical realizability of the problem. Finlayson et al. proposed that a surface color can be uniquely determined by assuming illumination colors form a straight line in an inverse-chromaticity space [6]. Although the theory is simple and elegant, the method is not practical. Finlayson et al. [7] and Marchant et al. [17, 18] introduced an idea to calculate illumination invariant values from colors under different illuminations. The invariant value is determined by the surface color and is derived by assuming that blackbody radiation approximates the illumination color. The fact that illumination invariant values can be derived implies that we may not be able to determine a unique surface color from illumination differences when two surface colors have the same invariant values. Later, Kawakami et al. showed the inherent difficulty of the problem [13], but also showed that Finlayson et al.'s method [6] becomes more practical [14] by combining the blackbody radiation with the illumination color model. However, the method [14] takes time and cannot always reach the global optimum, since it uses an iterative framework.

This paper brings a solution for estimating illumination colors with a single surface color. The paper explains four characteristics of illumination and surface color spaces, that can be fundamentally derived from plausible color range of outdoor illumination. Based on the characteristics, the method succeeds in combining the constraints for a surface and illumination colors, and the surface color is uniquely determined. While the key idea of the method is proposed elsewhere [12], the paper provides the justification of the color range. It is derived by statistics using the analytic sky model proposed by Preetham et al. [22], which calculates optimal parameters for the model of Perez et al [21]. The definition of the range is essential for the method. The paper also shows that the method becomes robust when multiple illuminations are used, since the range of colors effectively refines the estimated illumination colors. The method is thoroughly tested on a variety of images and is shown to provide great improvement over previous methods.

The rest of the paper is organized as follows: Section 2 describes image formation and the introduction of illumination and surface color spaces. Section 3 describes the characteristics of each color space. Section 4 describes the

978-1-4244-3991-1/09/$25.00 ©2009 IEEE

surface color estimation, based on specified characteristics. We provide experimental results and discussions in Sections 5 and 6, respectively. Finally, in Section 7, we conclude our paper.

2. Illumination space and surface color space

2.1. Image Formation

The image intensity of diffuse objects taken by a digital color camera can be described as:

$$I_c = \int_\Omega S(\lambda)E(\lambda)q_c(\lambda)d\lambda \tag{1}$$

where I_c is the sensor response (RGB pixel values), $S(\lambda)$ is the surface spectral reflectance, $E(\lambda)$ is the illumination spectral power distribution, q_c is the three-element vector of sensor sensitivity, and index c represents the type of sensors (R, G, and B). The integration is done over the visible spectrum (Ω). In this model, we assume that the output of camera response is linear to the flux of incoming light intensity, and ignore camera noise and gain.

Let us assume that the camera sensitivity function is sufficiently narrow (*narrow-band assumption*), so that it can be approximated by the Dirac delta function. Then, Eq. (1) can be simply rewritten as:

$$I_c = S_c E_c \tag{2}$$

where $S_c = S(\lambda_c)$ and $E_c = E(\lambda_c)$. Camera sensitivity can be obtained using a monochrometer and a spectrometer [28]. If camera sensitivity cannot be approximated by the Dirac delta function (narrowband sensor), we could apply camera sharpening algorithms [1]. The practicality of the assumption is discussed in Section 6.

Following [6], this paper defines chromaticity (or specifically *image* chromaticity) as:

$$i_r = \frac{I_R}{I_B} \quad , \quad i_g = \frac{I_G}{I_B} \tag{3}$$

The reason for using Eq. (3) is because the relation of Eq. (2) still holds in this color space:

$$i_c = s_c e_c \qquad c = \{r, g\} \tag{4}$$

where s_c and e_c correspond to the chromaticities of S_c and E_c. We call s_c surface chromaticity and e_c illumination chromaticity. In Eq. (3), either the red or green channel may be alternatively used as the denominator if the intensity of the blue channel is considerably low.

2.2. Illumination space and surface color space

Let us consider two color spaces that represent surface and illumination colors. We denote those spaces as s_r-s_g (*surface color*) and $1/e_r$-$1/e_g$ (*illumination*) spaces, and they are related, from Eq. (4), as follows:

$$\begin{bmatrix} s_r \\ s_g \end{bmatrix} = \begin{bmatrix} i_r^1 & 0 \\ 0 & i_g^1 \end{bmatrix} \begin{bmatrix} 1/e_r^1 \\ 1/e_g^1 \end{bmatrix}, \tag{5}$$

where $[i_r^1, i_g^1]^t$, $[e_r^1, e_g^1]^t$ and $[s_r, s_g]^t$ are image, illumination and surface chromaticities, respectively.

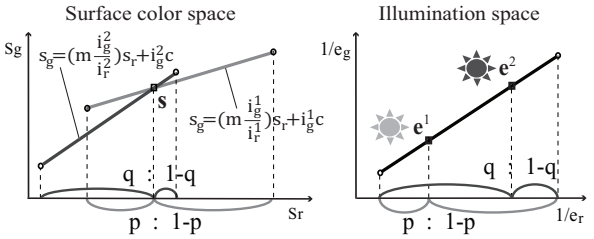

Figure 1. Two lines (Lines 1 and 2) in the surface color space are generated by $\mathbf{i^1} = [i_r^1, i_g^1]^t$ and $\mathbf{i^2}$. When the light color $\mathbf{e^1} = [e_r^1, e_g^1]^t$ divides the line in illumination space in $p : 1-p$, the surface color $\mathbf{s} = [s_r, s_g]^t$ divides Line 1 in $p : 1-p$, according to Eq. (5).

Why do we denote the illumination space in inverse chromaticity space? One reason is that *a simple scaling becomes the transformation between surface color and illumination spaces*, as shown in Eq. (5). The other is that we can utilize the assumption proposed by Finlayson et al. (see Figure 1 in the reference [6]): outdoor illumination colors can be approximated as a straight line in the illumination space, such as:

$$\frac{1}{e_g} = m\frac{1}{e_r} + c. \tag{6}$$

This is derived from the statistical knowledge of natural (outdoor) illumination distributions [6]. We verify the straight-line assumption in detail in 3.1.

3. Characteristics of the spaces

We can derive several characteristics of illumination and surface color spaces. They include key information to determine the surface color from multiple image chromaticities. The following summarizes the four important characteristics:

1. The straight line (Eq. (6)) in illumination space is not an infinite line, but a line segment. Accordingly, a line segment is spanned by an image chromaticity in surface color space, using Eq. (5).

2. Image chromaticities $\mathbf{i^1}, \cdots, \mathbf{i^n}$ from n illumination colors with a surface color generate line segments that intersect at the surface color $\mathbf{s} = [s_r, s_g]^t$ in surface color space.

3. When an illumination color $\mathbf{e^1} = [e_r^1, e_g^1]^t$ divides the line (Eq. (6)) in $p : p-1$ in illumination space, the surface color $\mathbf{s} = [s_r, s_g]^t$ divides the line segment generated from $\mathbf{i^1} = [i_r^1, i_g^1]^t$ in $p : p-1$ in surface color space. This is illustrated in Figure 1.

4. The input errors on each color component r and g effect differently in determining the surface color.

Based on those characteristics, the next section of the paper proposes a method that estimates colors using a single surface color. Details of each characteristic are described in the following subsections.

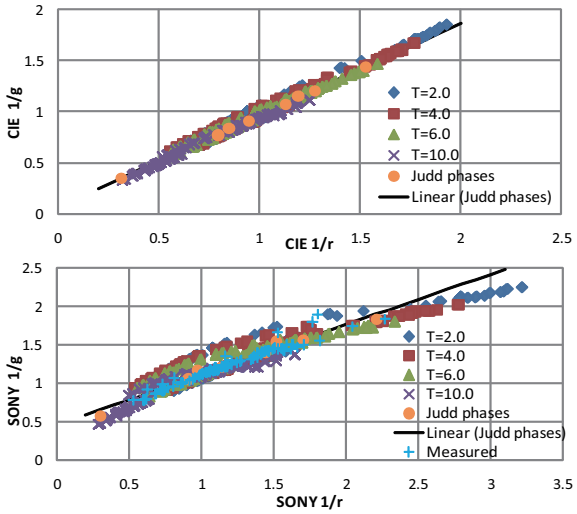

Figure 2. *Top:* Simulated CIE chromaticities of daylights in illumination space $(1/e_r, 1/e_g)$. Daylights have a specific range, and are tightly clustered around the straight line. *Bottom:* Simulated and measured chromaticities in SONY DXC-9000's illumination space. The model approximates the data quite well. The points are spread slightly, yet they are clustered around the same straight line. Similar results were obtained with different cameras' color spaces.

3.1. Characteristic 1: Finite range of outdoor illumination

Since the possible range of outdoor illumination colors is finite, the straight line (Eq. (6)) in illumination space is actually a line segment in the real world. This range of color temperatures varies from approximately 3500 to 12000 in Kelvin, according to the simulation and real data that we have obtained.

For the simulation, we used an analytic daylight model proposed by Preetham et al. [22]. The sky luminance in CIE (International Commission on Illumination) XYZ coordinates and the radiance of the sun are modeled by two parameters: turbidity and the sun direction. We tested four turbidities (2.0, 4.0, 6.0 and 10.0), and four zenith angles of the sun, ranged from 0.0 to 90.0 in degree by 30.0 degrees. The irradiance values are calculated at 60 different directions of a surface normal, that randomly distribute in the half of the hemisphere (the model is symmetric to the solar-antisolar meridian). We have also collected 111 irradiances of daylights measured at the rooftop deck of a building by using a white reflectance standard and a digital video camera, SONY DXC-9000.

The top figure in Figure 2 shows the plot of calculated irradiances in the illumination space $(1/e_r, 1/e_g)$, converted from the CIE XYZ values. Daylight colors have a specific range, and are tightly clustered around a straight line, which is the least square fit to the data of CIE standards and Judd's daylight phases (D48-D100). The bottom figure in Figure 2 shows the same plot in SONY DXC-9000's color space. To calculate RGB values in the camera's color space, we converted XYZ values into spectra [22], and then used Eq. (1). In the figure, we see that the model approximates the data quite well. The points are spread slightly, yet they are clustered around the same straight line. Thus, we determined the straight line to be the least square fit to the CIE standards and Judd's daylight phases.

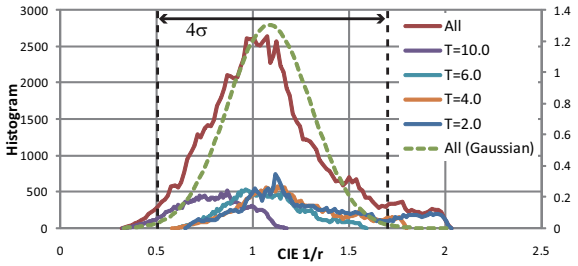

Figure 3. Probability distribution of daylights. The range shown in black dotted line covers the 4 σ range, and it corresponds to the range from 3500 to 12000 Kelvin in correlated color temperatures.

Figure 3 shows the probability distribution of daylight colors over the straight line. To obtain the figure, irradiances are generated using the sky model at 500 different surface normals (uniformly distributed) at every hour in solstice and equinox days. The cite was set to Washington D.C, America. Four turbidities aforementioned were used, and we assumed that they occur equally. Figure 3 shows each histogram obtained from each turbidity. The sum of the four histograms is shown in the red line. The correlated-color-temperature range from 3500 to 12000 in Kelvin has 4-σ probabilities of the all data. Thus, we set the straight line's range to be from 3500 to 12000 K in color temperatures.

Having defined a line segment in illumination space, another line segment can be generated in surface color space, accordingly. An image chromaticity spans a new line segment in surface color space, by using Eq. (5).

3.2. Characteristic 2: Constraint of multiple illuminations

Image chromaticities $\mathbf{i^1}, \cdots, \mathbf{i^n}$ of a surface $\mathbf{s}$ under n illuminations will generate n line segments in surface color space, by using Eq. (5). They will intersect at a unique point $\mathbf{s}$.

Proof: The line segment in surface color space, mapped by an image chromaticity $\mathbf{i} = [i_r, i_g]^t$ can be expressed as follows:

$$(mi_g/i_r)s_r - s_g = -i_g c, \tag{7}$$

from Eqs. (5) and (6).

Then, n image chromaticities will give a set of linear equations:

$$\begin{bmatrix} mi_g^1/i_r^1 & -1 \\ \vdots & \vdots \\ mi_g^n/i_r^n & -1 \end{bmatrix} \begin{bmatrix} s_r \\ s_g \end{bmatrix} = \begin{bmatrix} -i_g^1 c \\ \vdots \\ -i_g^n c \end{bmatrix} \tag{8}$$

Since image chromaticites $\mathbf{i^1}, \cdots, \mathbf{i^n}$ are different, any two of n equations are linearly independent to each other: By

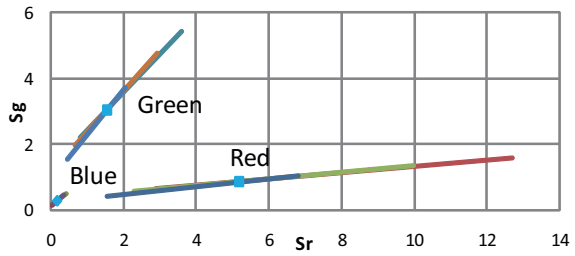

Figure 4. Multiple lines generated from image chromaticities in surface color space. The intersections are shown as blue points.

using any pair of image chromaticities, the surface color $\mathbf{s}$ is uniquely determined. Thus, the line segments expressed in Eq. (7) intersect at a single point, which is the surface color. This is consistent to the algorithm in [6], where the set of diagonal mappings that bring illumination change are assumed to have unique intersection when applied to image chromaticities.

Figure 4 shows the results of our simulation. We generated image chromaticities of red, green and blue surface colors, under ideal three illuminations. Each line segment intersects at a single point that is identical to the surface color. As shown Figure 4, the estimation is sensitive to input errors, as the lines almost coincide. The detailed description of the problem is stated in [14].

The surface color is estimated more robustly by increasing the number of illuminants, since Eq. (8) is over determined when three or more chromaticites are obtained. By combining the range of illumination colors with the multiple illumination constraint, the estimation finally becomes practical. The detailed algorithm is described in Section 4.

3.3. Characteristic 3: Ratio of line segment

Suppose that we have an image chromaticity $\mathbf{i^1} = [i_r^1, i_g^1]^t$, whose surface and illumination colors are $\mathbf{s} = [s_r, s_g]^t$ and $\mathbf{e^1} = [e_r^1, e_g^1]^t$. Let a line segment mapped by an image chromaticity $\mathbf{i^1}$ be Line 1. When the illumination color $\mathbf{e^1}$ internally divides the line segment in $p : 1-p$ in illumination space, the surface color $\mathbf{s}$ would be the point that divides Line 1 in $p : 1-p$, as illustrated in Figure 1. This is trivial from Eq. (5). The diagonal matrix expressed in Eq. (5) does not change the ratio of internal division.

This gives further constraints about the range of illumination colors, when multiple image chromaticites are available. Given two image chromaticities $\mathbf{i^1}$ and $\mathbf{i^2}$, we should observe two line segments intersecting, as illustrated in Figure 1. If they do not intersect, *it means that one or both illuminants are outside the range of outdoor illumination:* When the intersection $\mathbf{s}$ externally divides a line segment from $\mathbf{i^2}$ in $q : 1-q$, the illumination color $\mathbf{e^2}$ is the point that externally divides the illumination straight line in $q : 1-q$.

We can use this information for the reliability of illumination colors, since all the illumination colors should be in the defined range. The wider the colors of image chromaticities ($\mathbf{i^1}, \cdots, \mathbf{i^n}$) are, the more constraints we have. We will show how to combine the constraints with the determination of the surface color in the next section.

3.4. Characteristic 4: Effect of errors on each color component

An error on image chromaticity will map the straight line in illumination space to deviated position from it should be in surface color space.

The error results from sensor noises and systematic errors on inputs. Sensor noises include: read, quantization, dark current, and shot noises [19]. Systematic errors come from the discrepancy between the reality and the assumption: (1) the straight-line assumption for outdoor illumination colors, (2) the narrowband assumption that is only an approximation for general cameras, (3) the effect of the participating medium (air), (4) simple reflection models (objects may not be entirely diffuse), (5) interreflection, and (6) imperfect paintings or dust on surfaces.

We can derive how errors in each color component affect the determination of the surface color, by following the argument in [14] with a slight modification. When r component of image chromaticity (i_r^1) has an error ($\mathrm{d}i_r^1$), then the r component of surface chromaticity (s_r) is deviated to $s_r + \mathrm{d}s_{rr}$. Then, the error ratio $\mathrm{d}s_{rr}/s_r$ becomes [14];

$$\frac{\mathrm{d}s_{rr}}{s_r} = \frac{\mathrm{d}i_r^1}{\hat{i_r^1}} \frac{1}{1 - \left(1 + \frac{\mathrm{d}i_r^1}{\hat{i_r^1}}\right) \frac{i_r^1/i_g^1}{i_r^2/i_g^2}} \approx \frac{\mathrm{d}i_r^1}{\hat{i_r^1}} \frac{1}{1 - \frac{i_r^1/i_g^1}{i_r^2/i_g^2}} \tag{9}$$

from Eq. (8). Similarly, when i_g^1 has an error $\mathrm{d}i_g^1$, the error ratio becomes

$$\frac{\mathrm{d}s_{rg}}{s_r} \approx -\frac{\mathrm{d}s_{rr}}{s_r} \frac{\left(i_r^2 - i_r^1\right) i_g^2}{\left(i_g^2 - i_g^1\right) i_r^2} = -\frac{\mathrm{d}s_{rr}}{s_r} M \tag{10}$$

where $\mathrm{d}i_g^1/i_g^1$ is nearly equal to $\mathrm{d}i_r^1/i_r^1$. This shows that even the error ratios of i_r^1 and i_g^1 are the same, the effect on the estimation error ratio depends on the factor M. Similary, the same factor can be derived by using $\mathrm{d}s_g/s_g$.

4. Surface color estimation

Based on the characteristics, we designed a method that estimates a surface color from multiple image chromaticities. Instead of using Eq. (8), the method picks a pair of image chromaticity and finds the plausible illumination colors, such that the both colors exist on the line segment (Eq. (6) in illumination space. The method performs ${}_nC_2$ estimates from n image chromaticity, and the surface color is determined by taking the average of the ${}_nC_2$ surface colors. Estimated illumination colors are ensured to be inside the pre-set range in this approach.

For each pair of image chromaticities, the algorithm takes the following steps: (1) Estimate illumination colors. (2) If they are inside the range, store the surface color and go to the next pair. (3) Otherwise, find optimal input values that satisfy the constraint, and determine the illumination colors. (4) Store the surface color and go to the next pair.

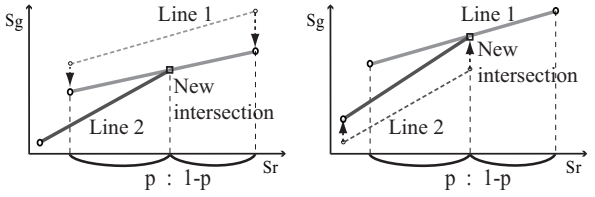

Figure 5. (a) The case of adjusting i_g^1. (b) The case of adjusting i_g^2. The ratio p does not change in either case.

When the estimated illumination colors are outside the range, the method tries to find an optimal solution, by finding plausible input values. Specifically, it selects one of the input chromaticity values and adjusts it, so that the intersection will be on both lines. Note that it estimates illumination colors from the ratio (p and q in Figure 1), instead of the intersection $\mathbf{s}$. Therefore, what matters is not the refined position but how the intersection divides the two lines.

Input image chromaticities consist of the four following values: i_r^1, i_g^1, i_r^2, and i_g^2. By adjusting one of them, we can move the intersection to be on both line segments. Selecting an input $\mathbf{i}^1$ or $\mathbf{i}^2$ makes no difference in illumination color estimation as shown in Figure 5. The left of Figure 5 is the case of selecting i_g^1, and the right is the case of selecting i_g^2. Whichever we adjust, i_g^1 or i_g^2, the new intersection would internally divide each line segment in the same ratio. The estimated results would be unchanged in both cases, as the ratio determines the illumination colors.

A slightly different estimation results depending on color components r or g. The method calculates the factor M in Eq. (10), and selects the one that has more effect. If M is larger than 1.0, a small difference in g affects the estimation more and vice versa.

5. Experimental results

We conducted experiments to evaluate the proposed method. First, we show the experimental results of using the GretagMacbeth color checker. Then, we show the results of using real outdoor scenes.

5.1. Color checker

Method Images of the GretagMacbeth ColorChecker were taken under six illuminants using SONY DXC-9000 progressive 3 CCD digital cameras by setting its gamma correction off. Images that were taken are shown in Figure 6. From Figure 6 (a) through (f), the color of the illuminant gradually changes from red to blue. The details of six illuminants are shown in Table 1. We have cut out each image of eighteen surface color patches, those surrounded by the red dotted line in Figure 6 (a), and prepared 18×6 color patch images. Each was resized to 70×70 pixels. We calculated the median RGB values of those pixels, and decided the image chromaticity of each image.

Having selected a pair of image chromaticities whose surface color is identical, we estimated their illumination chromaticities. The same was done with the previous methods [6, 14] for comparison. The total combination number of two illuminants and a surface was ${}_6C_2 \times 18 = 270$.

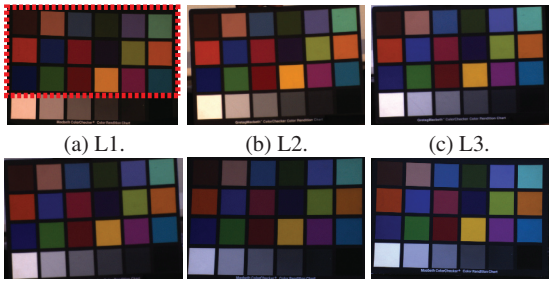

(a) L1. (b) L2. (c) L3.

(d) L4. (e) L5. (f) L6.

Figure 6. Images of the Macbeth ColorChecker taken under different outdoor illuminants (L1 to L6). Illuminant's color gradually changes from (a) to (f). Eighteen surface colors (colors surrounded by the red dotted line) were used in the experiments.

Table 1. Details of six illuminants used in the evaluation experiments.

Illuminants	**ID**	**CCT**[1] (K)
2003/8/22 17:30, Outdoor, Fine day	L1	3539
2007/3/16 16:30, Outdoor, Cloudy day	L2	4083
2003/3/16 15:30, Outdoor, Cloudy day	L3	5130
2003/3/16 13:00, Outdoor, Cloudy day	L4	5632
2003/7/14 14:30, Outdoor, Cloudy day	L5	5991
2003/7/14 18:20, Outdoor, Cloudy day	L6	7083

Results From the results of the 270 experiments, we show 30 selected results in Figure 7. Each row of the figure shows a pair of input images, estimated chromaticities (of two illuminants and a surface) obtained by the ground truth, the two previous methods [6, 14], and the proposed method. The figure includes (a) Red and (b) Blue surfaces. It is clear that the proposed method improves the previous methods' [6, 14] results. The bottom rows in each result show the average of the estimated surface colors by each method.

The averaged surface colors from each method are summarized in Figure 8. The top row shows the ground truth, and each column represents the 18 surface colors of the color checker. The second, third and bottom rows show the results from the previous [6, 14] and the proposed methods. We can see that if we take the average of the estimated surface colors, the results can be improved significantly. However, as shown in Figures 7 and 8, the estimates by the proposed method are more accurate than those of others.

In order to numerically evaluate our method, we calculated the average estimation errors of two illuminants and a surface. We defined the estimation error as the Euclidean distance between the estimated and true chromaticities in CIE LAB color space. The average estimation errors of the proposed method were 12.1 (redder illuminants $\mathbf{e}^1$), 12.2 (bluer illuminants $\mathbf{e}^2$) and 10.7 (surfaces.) Those of Finlayson et al.'s and Kawakami et al.'s methods [6, 14] were 16.4 and 13.7 (redder illuminants), 16.2 and 12.8 (bluer illuminants), and 14.0 and 11.9 (surfaces.) Note that the pre-

[1]Correlated Color Temperature.

Figure 8. Averaged surface colors from ${}_6C_2$ estimates. The top row (GT) shows the ground truth of the surface colors. The second (Fin95), third (Kaw05) and the bottom rows (Ours) show the estimated results using the previous [6, 14] and the proposed methods. We can see that if we take the average of the estimated surface color, the results can be improved significantly.

vious methods sometimes estimate negative color values. In the experiment, Finalyson et al.'s [6] and Kawakami et al.'s [14] methods produced 18 and 9 negative estimates, respectively. We excluded those cases from the color error evaluation, since we cannot define errors of negative values.

5.2. Real scenes

Method We have conducted experiments with real images; some of them are shown in Figure 9 (a). We used 19 images in total. They were taken in different times of the day; thus, they should include illumination color variations. An image can include multiple illuminations, since shadowed regions and non-shadowed regions are illuminated by different lights. The camera used was a digital still camera, Nikon D1. We set the gamma correction off to make sure that the camera responds linearly to the incoming light flux. Note that the gamma of Figure 9 is adjusted for display.

The pixels in images were classified by using the techniques in [7, 17, 14], which use illumination invariant value. Too bright/dark pixels were excluded from the process. The sky was also excluded from images, since it happened to have the same invariant value to that of the stones in images. The classified pixels are shown in Figure 9 (c). Each color corresponds to different illumination colors. The pixels in gray are the excluded pixels.

Chromaticities of illuminants were estimated by using the proposed method. The mean values of classified pixels were considered as the candidate values of (i_r, i_g). Having estimated illumination colors, we removed them from each pixel. We also averaged the intensity between classified regions; the average intensities of the regions in blue, cyan, yellow, magenta, and red in Figure 9 (c) are equivalent in Figure 9 (b).

Results The results are shown in Figure 9 (b). We can see that the color variance in Figure 9 (a) is removed in Figure 9 (b). We also compared the results with the Gray-world [3] and the White-patch [15] algorithms. Figure 10 (a), (b) and (c) show the results of Gray-world, White-patch, and the proposed algorithms, respectively. Estimated surface colors varies between images in Figure 10 (a) and (b), while they are uniform in Figure 10 (c).

6. Discussions

The errors due to the narrow-band assumption would be minor, because of the following reasons. First, it can be proved if the incoming spectrum and the spectral response are odd and even functions (or vice versa), then the narrow-band assumption becomes a perfect vehicle (see Proof 1). Second, even for the cases the assumption mentioned does not hold, the narrow-band assumption can be demonstrated to work by experiments with diverse surface reflectance, illuminations, and a few cameras (Proof 2). Third, much literature has shown that the assumption works for general cameras, such as in [1, 7, 17, 29].

Proof 1: Suppose that the camera sensitivity $G(\lambda)$ is a Gaussian:

$$G(\lambda) = k \exp(-(\lambda - \mu)^2/\sigma^2) \tag{11}$$

where μ is the center wavelength of the sensitivity, and k is a scaling factor. Let us suppose that the incoming spectrum $L(\lambda)$ is linear: $L(\lambda) = a(\lambda - \mu) + b$.

The narrow-band assumption holds, since we can prove the following equation:

$$\int L(\lambda)G(\lambda)d\lambda \ = mL(\mu) \ = mb. \tag{12}$$

where m is a factor irrelevant to the spectrum. The intensity captured by the camera only depends on $L(\mu)$, the spectral value at the center wavelength.

We will substitute $(\lambda - \mu)/\sigma$ with x for simplicity. Then, the left part of Eq. (12) becomes

$$\begin{aligned} &\int (a(\sigma x) + b)k \exp(-x^2)(\sigma dx) \\ &= -\frac{a\sigma^2 k}{2} \int (-2x) \exp(-x^2)dx + bk\sigma \int \exp(-x^2)dx \\ &= -\frac{a\sigma^2 k}{2} \left[\exp(-x^2)\right]_{-\infty}^{\infty} + bk\sigma\sqrt{\pi} = 0 + mb. \end{aligned} \tag{13}$$

Proof 2: From Eq. (4), we can derive the following equation:

$$\begin{bmatrix} 1/i_r \\ 1/i_g \end{bmatrix} = \begin{bmatrix} 1/s_r & 0 \\ 0 & 1/s_g \end{bmatrix} \begin{bmatrix} 1/e_r \\ 1/e_g \end{bmatrix}. \tag{14}$$

Thus, image chromaticities under different illumination colors should also form a straight line in the inverse-chromaticity space.

Figure 11 shows simulated chromaticities of a wide-band camera; they are generated from a number of daylight spectra, the Blue surface color of Macbeth ColorChecker, and the sensitivity of SONY DXC-9000. The figure shows that the simulated chromaticities still clustered around the ideal straight line. Thus, the errors caused by the narrow-band assumption should be limited to the difference of the actual and ideal chromaticities shown in Figure 11.

7. Conclusions

We have proposed a method that estimates colors using a single surface color. Four characteristics of illumination and surface color spaces were introduced: (1) the finite range of illumination colors, (2) what constraints multiple illuminations give, (3) what constraints the ratio of line segments give in the spaces, and (4) how each color component affect the estimation. The designed algorithm based on those characteristics successfully recovered the surface color.

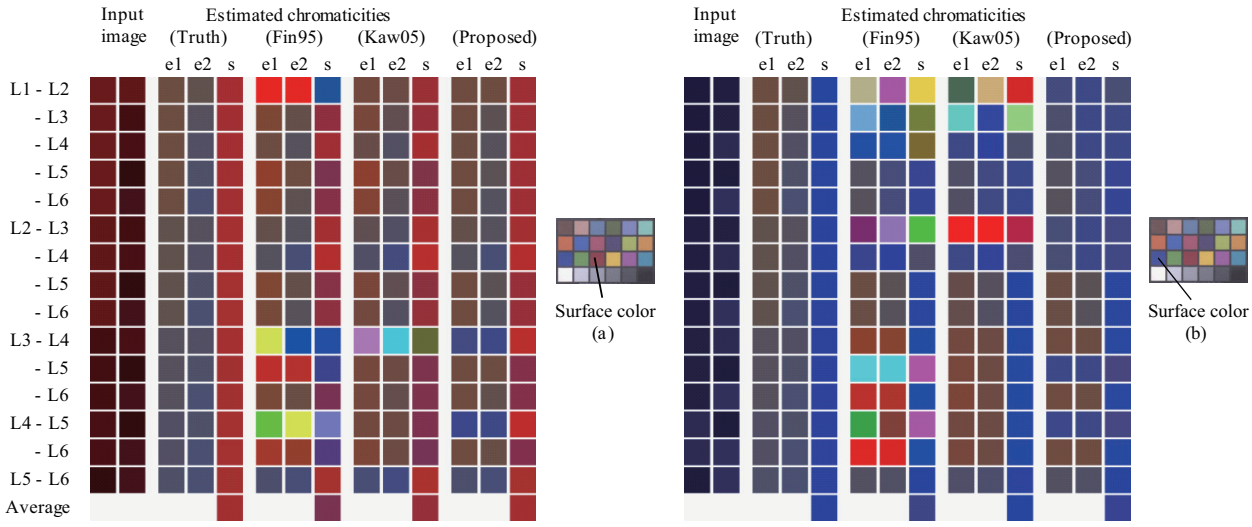

Figure 7. The figure shows the results of using (a) Red and (b) Blue of the Macbeth chart. Each row shows a pair of input images, estimated chromaticities (of two illuminants and a surface) obtained by the ground truth, the previous methods (Finlayson et al. ICCV 95 [6] and Kawakami et al. ICCV 05 [14]), and the proposed method. L1 to L6 are the outdoor illuminants that are used; there are ${}_6C_2 = 15$ rows for each surface color. The bottom rows show the average of the estimated surface colors by each method.

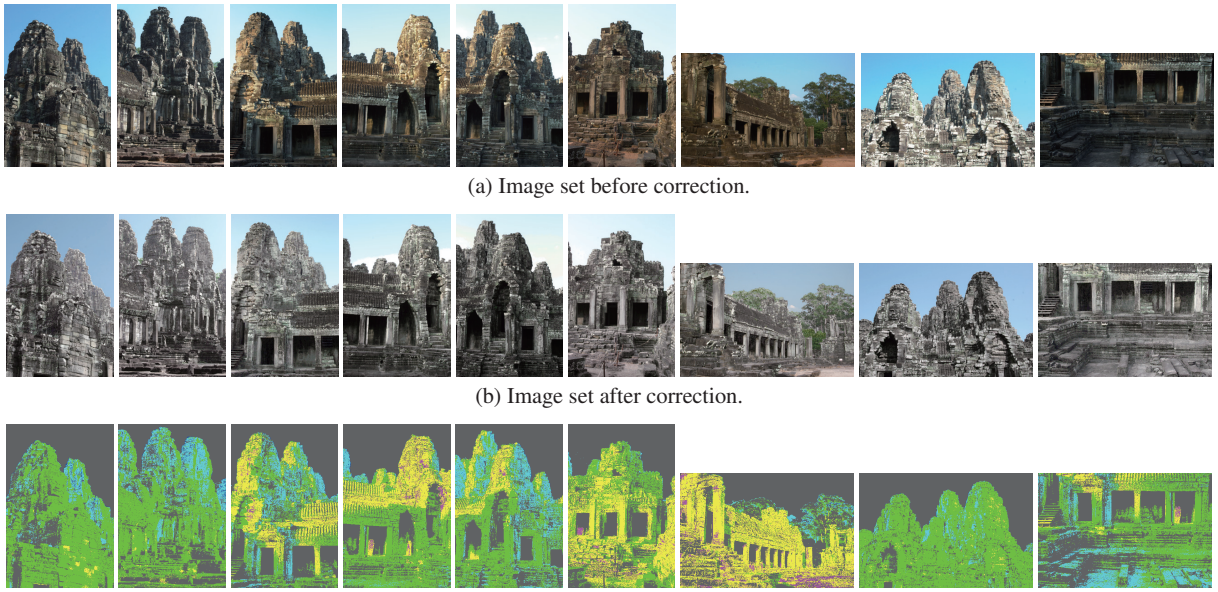

(a) Image set before correction.

(b) Image set after correction.

(c) Pixels classified to each illumination color.

Figure 9. Experimental results. (a) shows some of the images input to the method. (b) shows the results of illumination color removal of (a). (c) shows five groups where the pixels are classified. Each color represents different groups: blue, cyan, green, yellow, magenta (from the bluest).

Our next project is to make the method applicable to images with redundant colors. The problem of estimating consistent intensities between images also remains. We are planning to extract consistent intensities from images in varying illumination conditions.

Acknowledgement

This research was supported in part by the Ministry of Education, Culture, Sports, Science and Technology under the Leading Project, "Development of High Fidelity Digitization Software for Large-Scale andIntangible Cultural Assets." The authors would like to thank Joan Knapp for proofreading and editing this

(a) Gray world.

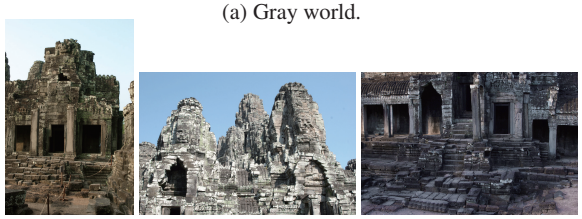

(b) White patch.

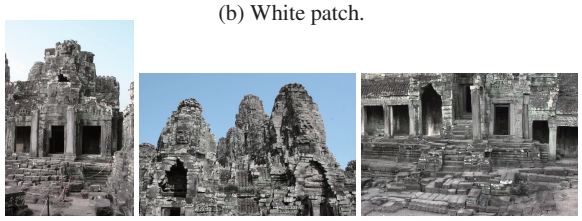

(c) Proposed.

Figure 10. Comparison between (a) Gray world, (b) White patch, and (c) the proposed methods. (c) displays the same images in Figure 9 (b).

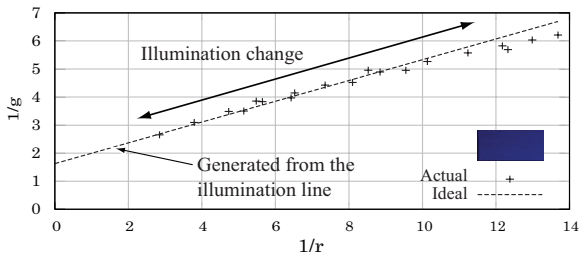

Figure 11. Simulated image chromaticities under illumination change: Actual (crosses) and ideal (lines) chromaticities in inverse-chromaticity. The figure shows the color change of the Blue surface of Macbeth ColorChecker. The used the sensitivity of SONY DXC-9000 (wide-band sensitivity) for the simulation.

manuscript. They also thank the anonymous reviewers for their careful reviews of the paper.

References

[1] K. Barnard, F. Ciurea, and B. Funt. Sensor sharpening for computational color constancy. *JOSA*, 18(11):2728–2743, 2001.

[2] D. H. Brainard and W. T. Freeman. Bayesian color constancy. *JOSA*, 14(7):1393–1411, 1997.

[3] G. Buchsbaum. A spatial processor model for object colour perception. *J. Franklin Institute*, 310(1):1–26, 1980.

[4] M. D'Zmura and P. Lennie. Mechanism of color constancy. *JOSA*, 3(10):1162–1672, 1986.

[5] G. Finlayson, S. Hordley, and I. Tastl. Gamut constrained illuminant estimation. *IJCV*, 67(1):93–109, 2006.

[6] G. D. Finlayson, B. V. Funt, and K. Barnard. Color constancy under varying illumination. In *Proc. ICCV*, pages 720–725, 1995.

[7] G. D. Finlayson and S. D. Hordley. Color constancy at a pixel. *JOSA*, 18(2):253–264, 2001.

[8] G. D. Finlayson, S. D. Hordley, and P. Hubel. Color by correlation: a simple, unifying, framework for color constancy. *PAMI*, 23(11):1209–1221, 2001.

[9] D. A. Forsyth. A novel algorithm for color constancy. *IJCV*, 5(1):5–36, 1990.

[10] A. Gijsenij and T. Gevers. Color constancy using natural image statistics. In *Proc. CVPR*, pages 1–8, 2007.

[11] S. Hordley. Scene illuminant estimation: past, present, and future. *Col. Res. Appl.*, 31(4):303–314, 2006.

[12] R. Kawakami and K. Ikeuchi. Stabilizing illumination chromaticity estimation using the illumination line segment. In *IAPR Conf. Mach. Vis. Appl. (MVA)*, May 2007.

[13] R. Kawakami, J. Takamatsu, and K. Ikeuchi. Color constancy from blackbody illumination. *JOSA*, 24(7):1886–1893, 2007.

[14] R. Kawakami, R. T. Tan, and K. Ikeuchi. Consistent surface color for texturing large objects in outdoor scenes. In *Proc. ICCV*, pages 1200–1207, 2005.

[15] E. Land. The retinex theory of color vision. *Scientific American*, 237(6):108–128, 1977.

[16] H. C. Lee. Method for computing the scene-illuminant from specular highlights. *JOSA*, 3(10):1694–1699, 1986.

[17] J. Marchant and C. Onyango. Shadow-invariant classification for scenes illuminated by daylight. *JOSA*, 17(11):1952–1961, 2000.

[18] J. Marchant and C. Onyango. Spectral invariance under daylight illumination changes. *JOSA*, 19(5):840–848, 2002.

[19] T. Mitsunaga and S. K. Nayar. Radiometric self calibration. In *Proc. CVPR*, pages 374–380, 1999.

[20] C. L. Novak and S. A. Shafer. Supervised color constancy for machine vision. In *Physics-based vision: Principles and practice, Color*, pages 284–299. Jones & Bartlett, 1992.

[21] R. Perez, R. Seals, and J. Michalsky. All-weather model for sky luminance distribution - preliminary configuration and validation. *Solar Energy*, 50(3):235–245, 1993.

[22] A. J. Preetham, P. Shirley, and B. Smits. A practical analytic model for daylight. In *Proc. SIGGRAPH*, pages 91–100, 1999.

[23] C. Rosenberg, M. Hebert, and S. Thrum. Color constancy using kl-divergence. In *Proc. ICCV*, pages 239–246, 2001.

[24] R. T. Tan, K. Nishino, and K. Ikeuchi. Color constancy through inverse intensity-chromaticity space. *JOSA*, 21(3):321–334, 2004.

[25] S. Tominaga and B. Wandell. Natural scene-illuminant estimation using the sensor correlation. *Proc. IEEE*, 90(1):42–56, 2002.

[26] S. Tominaga and B. A. Wandell. Standard surface-reflectance model and illuminant estimation. *JOSA*, 6(4):576–584, 1989.

[27] J. van de Weijer, T. Gevers, and A. Gijsenij. Edge-based color constancy. *Trans. Im. Proc.*, 16(9):2207–2214, 2007.

[28] P. L. Vora, J. E. Farrell, J. D. Tietz, and D. H. Brainard. Digital color cameras - 2 - spectral response. *HP-TR*, 1997.

[29] J. A. Worthey and M. H. Brill. Heuristic analysis of von kries color constancy. *JOSA*, 3(10):1708–1712, 1986.